Research Square

Preprints are preliminary reports that have not undergone peer review.
They should not be considered conclusive, used to inform clinical practice,
or referenced by the media as validated information.

Enhanced wear resistance of fine-grained Ni-based coating via annealing-induced phase transformation

Muhammad Arslan Hafeez
Huazhong University of Science and Technology
Jia-Xuan He
Huazhong University of Science and Technology
Zhang Cheng
czhang@mail.hust.edu.cn
Huazhong University of Science and Technology
Lin Liu
Huazhong University of Science and Technology

Research Article

Keywords: Ni-based coating, Annealing, Grain refinement, Ductile and hard phases, Wear resistance

Posted Date: July 24th, 2026

DOI: https://doi.org/10.21203/rs.3.rs-10329915/v1

License: This work is licensed under a Creative Commons Attribution 4.0 International License.
Read Full License

Additional Declarations: No competing interests reported.

Enhanced wear resistance of fine-grained Ni-based coating via annealing-induced phase transformation

Muhammad Arslan Hafeez[1], Jia-Xuan He, Cheng Zhang[1, *], Lin Liu[1, *]

[1]School of Materials Science and Engineering, State Key Lab for Materials Processing and Die & Mold Technology, Huazhong University of Science and Technology, Wuhan 430074, China

**Corresponding authors: czhang@mail.hust.edu.cn* and *lliu2000@mail.hust.edu.cn*

Abstract

Annealing is widely applied to reduce porosity and enhance the wear resistance of thermally sprayed metallic coatings; however, its effectiveness is often limited by grain coarsening and brittle phase formation. Here, we present a new approach that directly overcomes these limitations by coupling thermal spraying with the crystallization behavior of a rationally designed amorphous alloy powder ($Ni_{68.6}Cr_{8.7}Nb_3P_{16}B_{3.2}Si_{0.5}$). Upon annealing at 800 °C for 1 h, the metastable $Mg_6Cu_{17}Si_7$-type phase present in the as-sprayed coating transforms into a well-refined three-phase microstructure, comprising a ductile Ni-based solid solution and hard Ni_3P and $NbNi_3$ intermetallic phases, with 51% reduced intersplat density. This microstructural configuration results in a 21% reduction in COF and an 89% reduction in wear rate. The worn surface of annealed coating demonstrates minor thin grooves, lower fractions of oxides, and no sign of spallation, delamination or cracking, presenting a significant improvement in the wear resistance after annealing. This improvement originates from the three-phase composite microstructure in which the ductile Ni-based solid solution provides plastic deformability and crack resistance, whereas the hard Ni_3P and $NbNi_3$ phases provide hardness and load-bearing capacity. Annealed coating exhibits mild abrasive wear mechanism coupled with limited plastic deformation. These findings demonstrate that

controlled crystallization of thermally-sprayed coatings can be used to engineer beneficial phases, providing a promising strategy for the design of high-performance wear-resistant coatings.

Keywords: Ni-based coating; Annealing; Grain refinement; Ductile and hard phases, Wear resistance

1. Introduction

In modern industries such as aerospace, automotive, marine, energy, mining, and tooling, abrasive wear of mechanical components is a major concern, causing material loss, equipment failures, higher maintenance costs, and reduced service life [1, 2]. The high-velocity oxy-fuel (HVOF)-sprayed amorphous metallic coatings (AMCs) have attracted increasing attention for demanding wear applications in last two decades [3, 4]. However, their metastable nature and HVOF-induced defects, such as porosity, intersplat voids, oxide stringers, and partial crystallization, reduce load-bearing capacity and limit tribological performance [5]. To address these issues, post-spray treatments including sealing [6], shot peening [7], laser re-melting [8], and annealing treatment [9] have been widely employed.

Annealing is one of the extensively used post-spray treatment for reducing HVOF-induced defects in AMCs and improving their tribological performance [10]. Several studies have explored its effects on wear behavior. Yang et al. [11] reported that annealing FeCrAlTiMo AMCs at 850 °C enhanced hardness, bonding strength, and wear resistance due to the precipitation of multiple hard phases. Abbas et al. [12] observed similar improvements in FeCrMoCBY AMCs annealed at 700 °C, attributed to the formation of hard M_xC_γ carbides along crystallite boundaries. Cheng et al. [13] demonstrated that annealing promoted Fe_3B, $Fe_{23}B_6$, and α-Fe phase precipitation, increasing hardness, Young's modulus, and wear resistance in FeBSiNb AMCs. Liu et al. [14] also found that Fe-based AMCs annealed at 700–900 °C exhibited significantly superior wear resistance compared with the as-sprayed counterparts.

Nevertheless, the extent of wear resistance enhancement in AMCs by annealing treatment is often constrained by its adverse effects, such as formation of brittle intermetallics due to crystallization, or the development of mechanically unstable tribo-oxide layers, especially when the amorphous

alloy is not supportive or the annealing process is not carefully optimized [15, 16]. Consequently, these limitations underscore the need to develop new amorphous alloy systems and to precisely control annealing parameters to minimize these adverse effects through fully controlled phase transformations [17]. Full wear-resistance potential of annealed AMCs can only be realized through the synergistic optimization of alloy composition and annealing treatment [18]. Compared with extensively investigated Fe-based AMCs [19-22], Ni-based AMCs have received limited attention despite their attractive combination of mechanical strength, tribological performance, and electrochemical stability [23-26]. This is largely due to their weak glass forming ability, low resistance to crystallization, and tendency to form brittle intermetallic phases during annealing [27-29]. Furthermore, the inherent complexity associated with optimizing Ni-based alloy compositions and annealing parameters to achieve a structurally stable, defect-minimized, and wear-resistant microstructure has hindered systematic investigations and remains a critical challenge [30, 31].

To address this challenge, a wear-resistant fine-grained Ni-based coating was developed through a systematic optimization of composition and annealing strategy. In this study, a specially designed $Ni_{68.6}Cr_{8.7}Nb_3P_{16}B_{3.2}Si_{0.5}$ amorphous alloy was selected, and its amorphous powder was deposited onto an AISI 1045 steel substrate using the HVOF technique. Following deposition, the coating was annealed at an optimized temperature of 800 °C for 1 h to precisely control phase transformations and effectively mitigate spray-induced defects. The annealing treatment triggered a controlled three-step crystallization process, resulting in a fine-grained composite microstructure composed of a ductile Ni-based solid-solution phase, a hard Ni_3P intermetallic phase, and a trace amount of $NbNi_3$ intermetallic phase. The annealing treatment also minimized the intersplat voids and, importantly, significantly refined the grain size due to the phase transformation. This dense,

refined and well-balanced microstructure significantly enhanced coating hardness and imparted outstanding wear resistance, surpassing that of conventional Fe-based, Cr-based, Ni-based, Co-based, Cr_3C_2-based, and WC-reinforced amorphous and/or crystalline coatings. Consequently, the developed coating demonstrates strong potential for application in demanding wear environments.

2. Experimental procedure

2.1.Materials, coating preparation, and annealing process

A novel $Ni_{68.6}Cr_{8.7}Nb_3P_{16}B_{3.2}Si_{0.5}$ (at. %) amorphous powder, custom designed especially for this study, was obtained from Beijing Sun Spraying New Material Co., Ltd. of China and used as feedstock. AISI 1045 steel was selected as the substrate due to its widespread use in engineering applications. The coatings were deposited using an HVOF-spraying system (UniCoatPro–WokaStar 610s, Oerlikon Metco, USA) and subsequently annealed at 800 ℃ for 1 h in a vacuum furnace followed by natural cooling in ambient air. The powder characteristics, HVOF spraying procedure and process parameters, and optimization of subsequent annealing treatment are comprehensively investigated in our previous work [32].

2.2.Morphological and microstructural analyses of the coatings

The microstructural characteristics of the as-sprayed and annealed $Ni_{68.6}Cr_{8.7}Nb_3P_{16}B_{3.2}Si_{0.5}$ coatings were investigated using cross-sectional samples prepared by cutting, grinding, and polishing, followed by examination with a scanning electron microscope (SEM, FEI Quanta 650 FEG, USA) using 20 kV acceleration voltage and backscattered electron detector (BSED). To assess the effect of annealing on coating densification, intersplat density was quantitatively analyzed from high-magnification cross-sectional SEM micrographs using Image-Pro Plus 6.0 software. Annealing-induced phase transformation was analyzed by X-ray diffraction (XRD)

analysis on an X-ray diffractometer (Shimadzu XRD-7000, Japan). To further elucidate the annealing-induced phase transformation and grain refinement, transmission electron microscopy (TEM, Talos F200X G2, USA) was employed. For TEM sample preparation, the coatings were mechanically detached from the substrate, grounded to approximately 30 μm, and subsequently ion-milled (Gatan Model 695 system (USA)) to electron transparency. For grain size analysis, five TEM images were used for each phase and the final value was determined by averaging the ten measurements.

2.3.Tribological analysis

To evaluate the wear resistance of as-sprayed and annealed $Ni_{68.6}Cr_{8.7}Nb_3P_{16}B_{3.2}Si_{0.5}$ coatings, dry sliding wear tests were conducted in reciprocating mode. Coated samples with dimensions of 10 mm × 10 mm × 5.38 mm were prepared by grinding and polishing according to the aforementioned procedure. The wear tests were performed on a ball-on-disk tribometer (Bruker, UMT-TL, China) at a sliding speed of 10 mm/s and a sliding amplitude of 3 mm for 30 min under an applied load of 20 N at room temperature. Commercial Si_3N_4 balls with a diameter of 6.35 mm were used as the counterbody, and a new ball was used for each test. Three tests were conducted for each coating to ensure data reliability and reproducibility.

2.4.Worn surface characterizations

To observe the three-dimensional profile and measure the dimensions of the wear tracks, a white light interferometer (Zygo, NewView 8300, USA) was employed. The microscale features of the wear tracks from both top surface and cross-section were further examined using a SEM equipped with EDS. The chemical composition and oxidation states of the elements within the oxide films formed during the wear test were analyzed using X-ray photoelectron spectroscopy (XPS, Kratos

Analytical Ltd., DLD-600W, USA). The instrument was equipped with a monochromatic Al Kα radiation source and operated under ultrahigh vacuum conditions (2.0×10^{-9} bar). Prior to data acquisition, surface contaminants were removed by Ar^+ ion sputtering for 40 s. Binding energies were calibrated using the C 1s peak at 285.0 eV. Spectral deconvolution and quantitative analysis were performed using XPSPEAK software with linear background subtraction, allowing accurate determination of elemental distributions and chemical states within the passive films.

3. Results and discussion

3.1.Microstructures

Fig. 1 presents cross-sectional SEM micrographs of the as-sprayed and annealed fine-grained $Ni_{68.6}Cr_{8.7}Nb_3P_{16}B_{3.2}Si_{0.5}$ coatings. The as-sprayed coating, with an average thickness of approximately 380 μm, exhibits layered structure with several pores and intersplats. As shown in Fig. 1(a) and (c), a typical lamellar morphology characteristic of thermal spray deposition is observed, featuring well-defined intersplat boundaries and numerous microvoids. After annealing at 800 °C for 1 h, significant microstructural consolidation occurs, as evidenced by a pronounced reduction in porosity and intersplat boundaries. Only faint remnants of the original lamellar architecture remain visible in the annealed coating (Fig. 1(b) and (d)). This densification is further corroborated by a ~51% reduction in intersplat density from 0.088 ± 0.004 to 0.043 ± 0.002 μm^{-2} following annealing.

The insets in Fig. 1(a) and (b) show the corresponding XRD patterns of the as-sprayed and annealed coatings. In contrast to the amorphous feedstock powder [32], the as-sprayed coating exhibits a crystalline structure, which is attributed to the high thermal input during the HVOF spraying process. The dominant crystalline phase in the as-sprayed coating is identified as an FCC $Mg_6Cu_{17}Si_7$-type phase, accompanied by minor fractions of tetragonal Ni_3P and FCC Ni-based

solid solution phases. Upon annealing at 800 °C for 1 h, the primary $Mg_6Cu_{17}Si_7$-type phase decomposes, resulting in a three-phase microstructure consisting of an FCC Ni-based solid solution phase, a tetragonal Ni_3P intermetallic phase, and trace amount of orthorhombic $NbNi_3$.

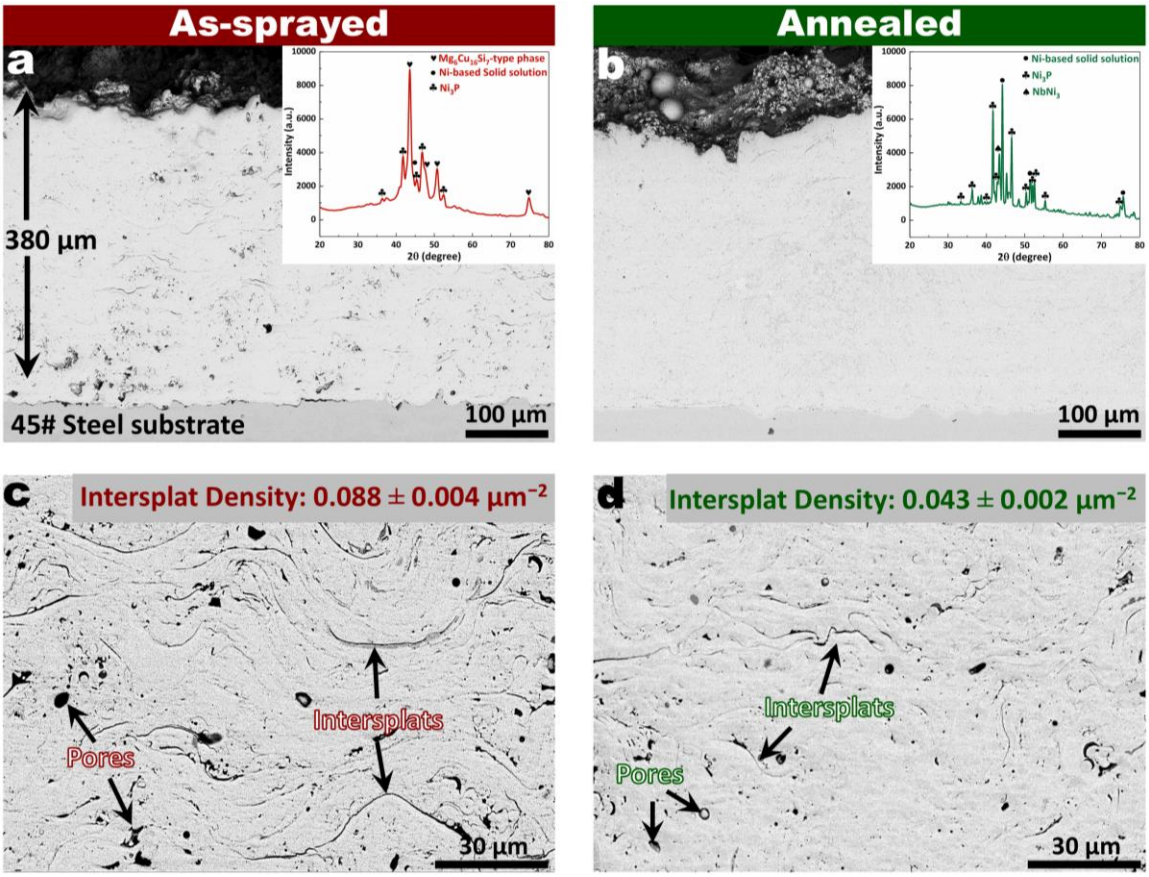


Fig. 1. Backscattered SEM micrographs (cross-sectional) of the fine-grained $Ni_{68.6}Cr_{8.7}Nb_3P_{16}B_{3.2}Si_{0.5}$ coatings: **(a)** and **(c)** as-sprayed and **(b)** and **(d)** annealed coatings. The insets in **(a)** and **(b)** show the corresponding XRD patterns of the as-sprayed and annealed coatings, respectively.

To further elucidate the microstructural characteristics and validate the annealing-induced phase transformations, TEM analysis was performed on both coatings (i.e., as-sprayed and annealed) and the obtained bright-field (BF) TEM images and corresponding selected area electron diffraction (SAED) patterns are depicted in Fig. 2. A BF-TEM image and the associated SAED patterns confirms the crystalline nature of the as-sprayed coating. The primary phase in as-sprayed coating

is indexed as an FCC $Mg_6Cu_{17}Si_7$-type intermetallic phase (Composition: $Ni_{72.4}Cr_{10.3}Nb_{2.1}P_{14}Si_{0.9}$ (at. %)) with some fractions of Ni_3P intermetallic phase (Fig. 2(a)).

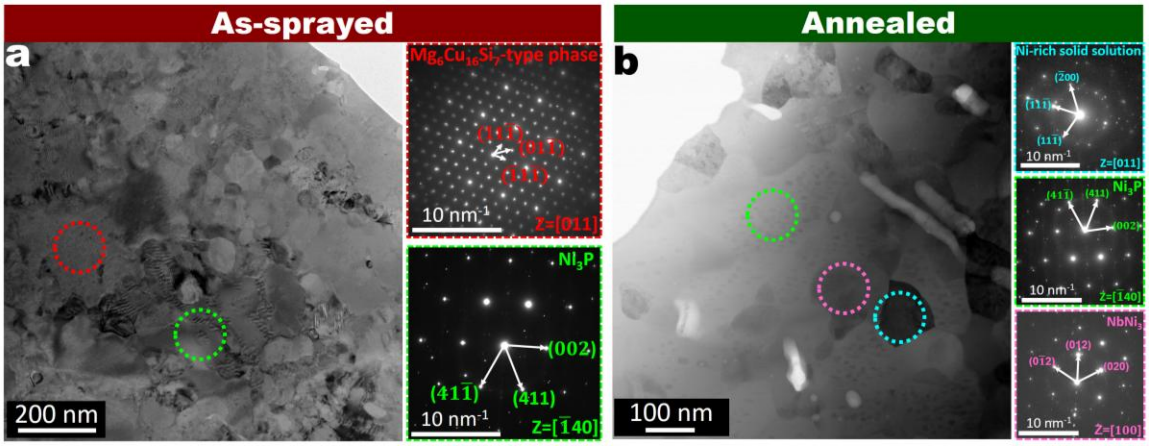


Fig. 2. BF-TEM micrograph and corresponding SAED patterns of **(a)** as-sprayed and **(b)** annealed fine-grained $Ni_{68.6}Cr_{8.7}Nb_3P_{16}B_{3.2}Si_{0.5}$ coating.

For the annealed coating, the BF-TEM image combined with SAED patterns reveals three distinct phases. The first phase is FCC Ni-based solid solution enriched in Ni and Cr (Composition: $Ni_{87.7}Cr_{9.6}Nb_{2.2}P_{0.2}Si_{0.2}$ (at. %)) and the second phase is a tetragonal Ni_3P phase enriched in P (Composition: $Ni_{74.7}Cr_{6.4}Nb_{0.4}P_{17}Si_{1.6}$ (at. %)) with minor fraction of orthorhombic $NbNi_3$ phase enriched in Nb (Composition: $Ni_{84.1}Cr_{2.3}Nb_{10.8}P_{1.7}Si_{1.1}$ (at. %)) (Fig. 2(b)). These findings validate that the $Mg_6Cu_{17}Si_7$-type intermetallic phase in the as-sprayed coating decomposes into Ni-based solid solution, Ni_3P, and $NbNi_3$ phases after annealing, consistent with the XRD results (Fig.1).

Furthermore, the TEM-based grain size analysis reveals that the as-sprayed coating exhibits a coarse-grained microstructure with average grain size of 903 nm (Fig. 3(a)–(c)). The high-temperature annealing four-times refines the grain size providing an average grain size of 210 nm (Fig. 3(d)–(f)). The volume fractions of all phases in both coatings are comprehensively explained in our previous work [32].

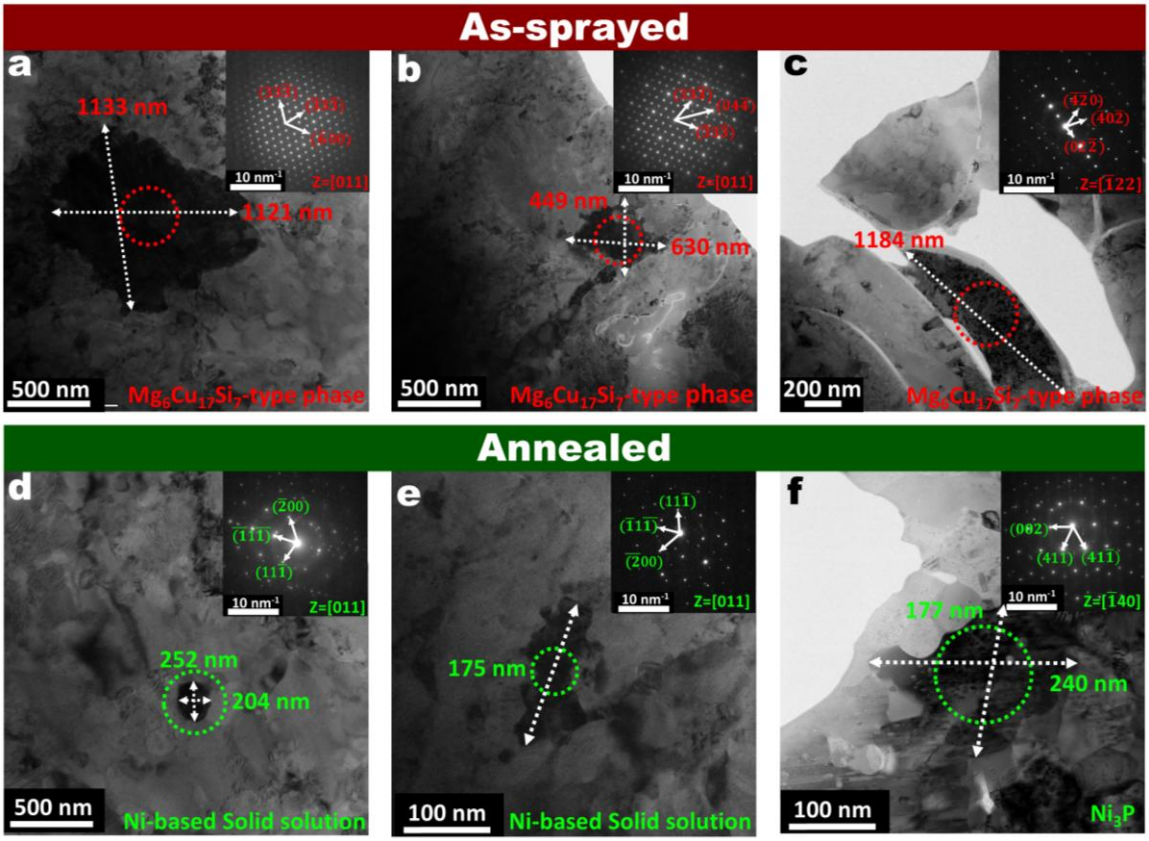


Fig. 3. TEM images and corresponding SAED patterns showing the grain sizes of as-sprayed: **(a)–(c)** $Mg_6Cu_{16}Si_7$-type intermetallic phase; and annealed: **(d)–(e)** Ni-based solid solution phase and **(f)** Ni_3P phase, fine-grained $Ni_{68.6}Cr_{8.7}Nb_3P_{16}B_{3.2}Si_{0.5}$ coatings.

3.2.Tribological properties

Since hardness is a key parameter governing the tribological performance of thermally sprayed coatings, the annealing-induced increase in hardness from 795 ± 40 $HV_{0.1}$ to 921 ± 75 $HV_{0.1}$, coupled with the formation of a refined multiphase microstructure, is anticipated to improve the wear resistance of the $Ni_{68.6}Cr_{8.7}Nb_3P_{16}B_{3.2}Si_{0.5}$ coating. To verify this hypothesis, the tribological properties of the as-sprayed and annealed coatings were systematically evaluated under reciprocating dry-sliding conditions at room temperature using a Si_3N_4 ball as the counterbody. Fig. 4 presents the COF curves, the wear track dimensions, and 3D wear track morphologies. The as-sprayed coating exhibits an average COF of 0.73 ± 0.05, whereas the annealed coating

demonstrates improved frictional stability and a 21% lower COF value (0.43 ± 0.04), indicating enhanced wear resistance after annealing (Fig. 4(a)). The depth–width profiles and 3D wear track morphologies reveal significantly wider and deeper wear track of as-sprayed coating with a depth of 2.91 μm and a width of 359.33 μm (Fig. 4(b) and (c)). Conversely, the annealed coating exhibits a comparatively narrower and shallower wear track, with a depth of 0.47 μm and a width of 229.11 μm, highlighting its markedly improved wear resistance relative to the as-sprayed coating (Fig. 4(b) and (d)).

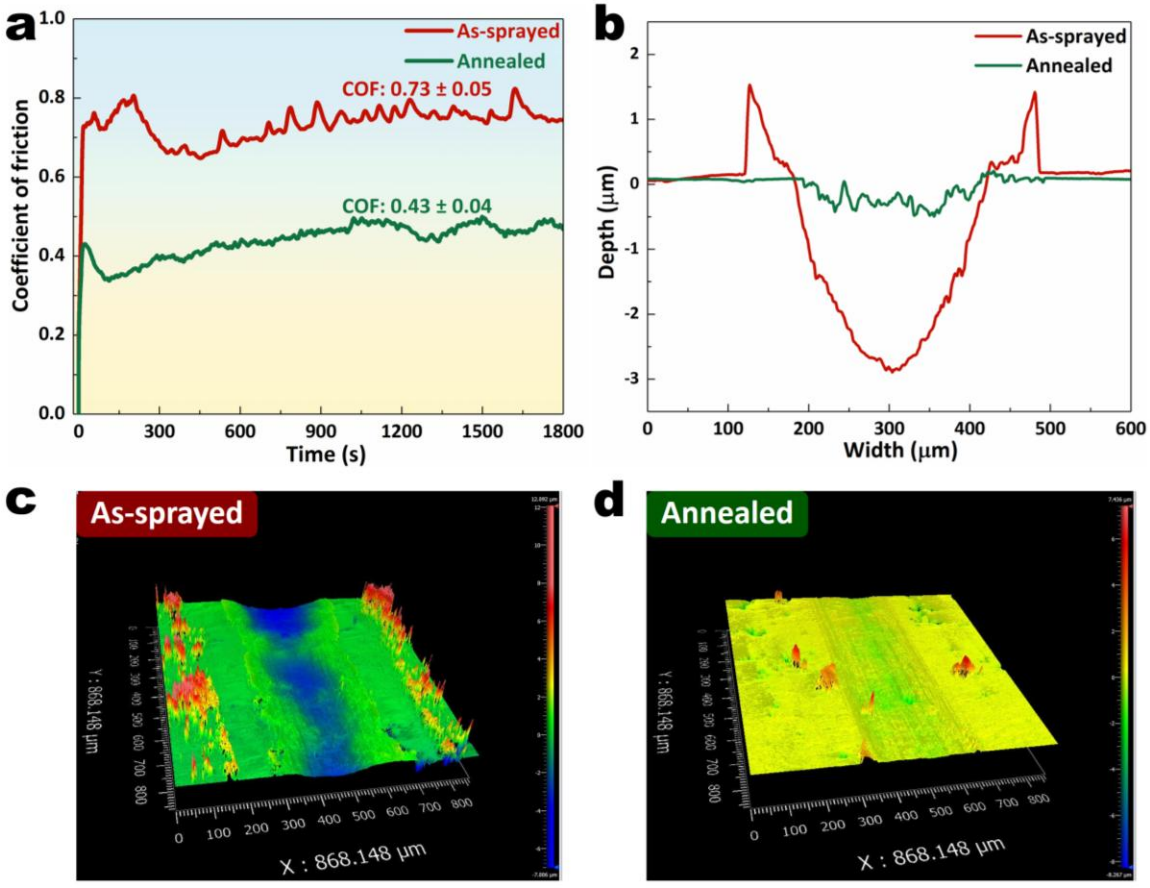


Fig. 4. (a) Plots of COF as a function of sliding time, **(b)** depth–width profiles of the wear tracks for the as-sprayed and annealed fine-grained $Ni_{68.6}Cr_{8.7}Nb_3P_{16}B_{3.2}Si_{0.5}$ coatings. Three-dimensional wear track morphologies of the **(c)** as-sprayed and **(d)** annealed fine-grained $Ni_{68.6}Cr_{8.7}Nb_3P_{16}B_{3.2}Si_{0.5}$ coatings.

The wear volumes and wear rates of both coatings were calculated from the wear track dimensions and are plotted in Fig. 5. The as-sprayed coating exhibits a relatively high wear volume of 4.70 ± 0.23 × 10^{-3} mm^3 and a wear rate of 17.79 ± 0.89 × 10^{-6} mm^3 $N^{-1}m^{-1}$. In contrast, the annealed coating shows an approximately 89% reduction in wear volume and wear rate, with values of 0.36 ± 0.02 × 10^{-3} mm^3 and 2.0 ± 0.10 × 10^{-6} mm^3 $N^{-1}m^{-1}$, respectively (Fig. 5).

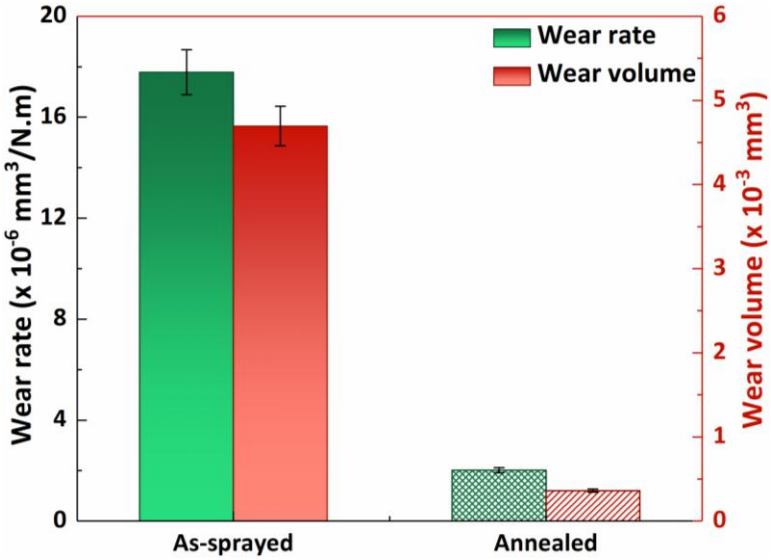


Fig. 5. Wear rates and wear volumes of the as-sprayed and annealed fine-grained $Ni_{68.6}Cr_{8.7}Nb_3P_{16}B_{3.2}Si_{0.5}$ coatings.

3.3.Structural characteristics of worn surfaces

The detailed structural characteristics of the worn surfaces of the as-sprayed and annealed coatings were evaluated from both top surface and cross-section, and the obtained SEM micrographs and EDS maps are presented in Figs. 6 and 7. The worn surface of the as-sprayed coating exhibits a relatively wide wear track and pronounced deep grooves, along with the presence of discrete oxide blocks, indicating significant tribo-oxidation during sliding (Fig. 6(a)). Higher magnification SEM images and associated EDS map further reveal extensive spallation regions and fragmented oxide debris distributed across the wear track (Fig. 6(c) and (e)). These oxide blocks, formed through

repeated rupture and delamination of a poorly adherent tribo-oxide film, fail to provide effective lubrication during sliding. Instead, they act as third-body abrasive particles, exacerbating surface damage. The combined presence of deep grooves, oxide debris, and spallation zones suggests that the wear mechanism of the as-sprayed coating is governed by a synergistic interplay of abrasive and adhesive wear, which accounts for its higher COF and wear rate.

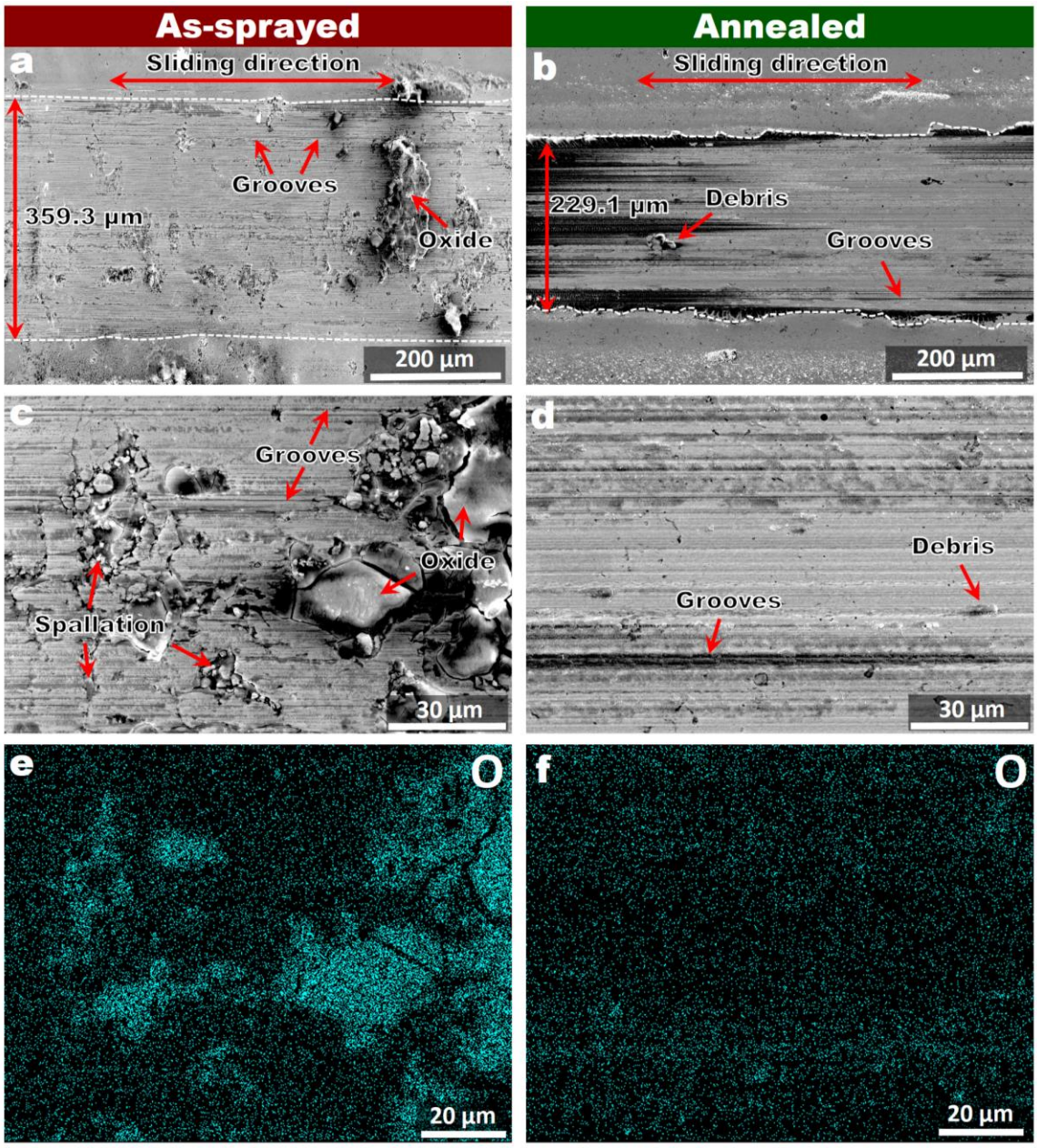


Fig. 6. Worn surface characteristics (top surface) of the as-sprayed: **(a)** and **(b)** SEM morphologies and **(c)** the corresponding EDS maps; and annealed: **(d)** and **(e)** SEM morphologies and **(f)** the corresponding EDS maps; fine-grained $Ni_{68.6}Cr_{8.7}Nb_3P_{16}B_{3.2}Si_{0.5}$ coating.

In contrast, the annealed coating demonstrates a markedly improved wear response, as evidenced by a significantly narrower wear track. The worn surface is characterized by shallow, uniformly distributed grooves with no evident oxide block formation or severe spallation (Fig. 6(b)), indicating a more stable tribological behavior under the applied load. Even at higher magnifications, SEM observations and EDS analysis reveal the absence of substantial oxidative damage or delamination features (Fig. 6(d) and (f)). Consequently, the wear mechanism in the annealed coating is predominantly governed by mild abrasive wear, which accounts for its significantly lower COF and wear rate.

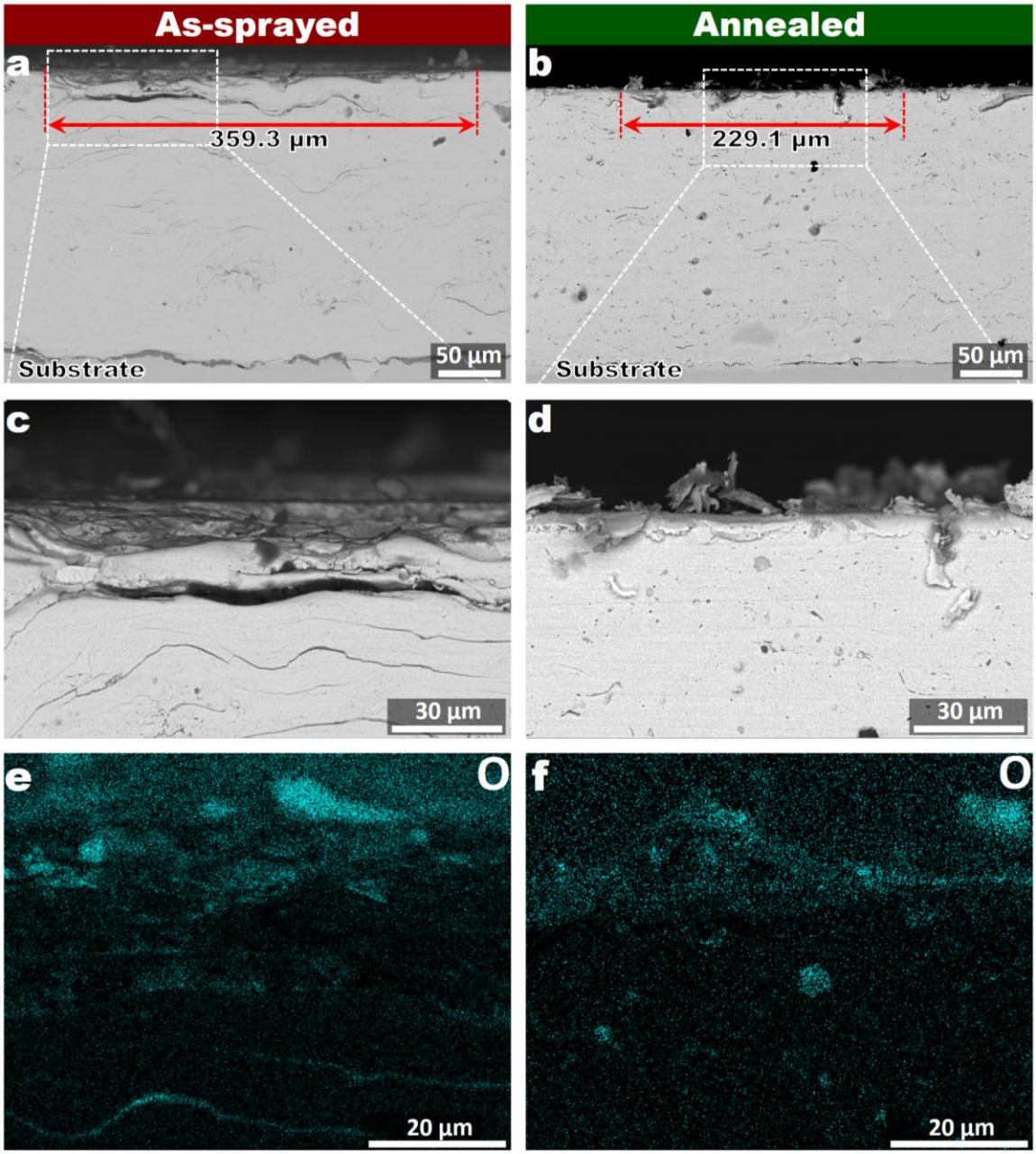


Fig. 7. Worn surface characteristics (cross-section) of the as-sprayed: **(a)** and **(b)** SEM morphologies and **(c)** the corresponding EDS maps; and annealed: **(d)** and **(e)** SEM morphologies and **(f)** the corresponding EDS maps; fine-grained $Ni_{68.6}Cr_{8.7}Nb_3P_{16}B_{3.2}Si_{0.5}$ coating.

To further evaluate the worn surface characteristics of the two coatings, cross-sectional SEM analysis of the wear tracks was carried out (Fig. 7). The as-sprayed coating exhibits severe subsurface wear damage, characterized by extensive material removal, a wide and deep wear scar, crack initiation and propagation along intersplats, and spallation of the intersplat voids beneath the

worn surface (Fig. 7(a) and (c)), and a partially developed oxide layer (Fig. 7(e)). This behavior indicates unstable tribological performance, driven by weak intersplat cohesion and localized stress concentration during sliding. In contrast, the annealed coating shows a markedly improved subsurface worn morphology with minimal material loss, a narrower and shallower wear track, and no crack formation or intersplat spallation near the wear interface (Fig. 7(b) and (d)). The oxide layer is thin and discontinuous, suggesting a significant reduction in oxidative wear (Fig. 7(f)). Overall, this further evaluation clearly demonstrates that annealing improves the microstructural integrity and subsurface damage resistance of the Ni-based coating, leading to superior anti-wear performance.

3.4.Compositional characteristics of worn surfaces

To evaluate the compositional characteristics of worn surface of the as-sprayed and annealed Ni-based coatings, XPS analysis was performed after wear testing. The XPS spectra of both the as-sprayed and annealed coatings reveal dominant signals corresponding to Ni, Cr, Nb, and P. Fig. 8 presents the high-resolution fitted XPS spectra of the Ni 2p, Cr 2p, Nb 3d, and P 2p core levels. For both coatings, the Ni 2p core-level spectra exhibit contributions from Ni^{0} (metallic Ni) and Ni^{2+} (NiO) at ~852.9 eV and ~856.0 eV, respectively (Fig. 8(a) and (e)). Similarly, the Cr 2p spectra reveal contributions from Cr^{0} (metallic Cr), Cr^{3+} (Cr_2O_3), and Cr^{6+} (CrO_3) at ~574.2 eV, ~577.0 eV, and ~579.0 eV, respectively, in both coatings [33] (Fig. 8(b) and (f)). Furthermore, the Nb 3d spectra of both coatings are resolved into two peaks at ~203.4 eV and ~207.5 eV, corresponding to Nb^{2+} (NbO) and Nb^{5+} (Nb_2O_5), respectively (Fig. 8(c) and (g)). P is a major constituent and plays a significant role in enhancing the wear resistance of the annealed Ni-based coating. The P 2p core-level spectra of both coatings are deconvoluted into two main peaks corresponding to P^{3-} (Ni_3P) at ~129.5 eV and P^{5+} (P_2O_5) (Fig. 8(d) and (h)). It is noteworthy that the presence of Ni^{0} and Cr^{0}

signals in the XPS spectra most likely originates from the Ni-based solid solution and Ni_3P phase in both coatings [34]. Furthermore, Nb^0 is not detected in the spectra, primarily due to the low fraction of Nb in the base alloy ($Ni_{68.6}Cr_{8.7}Nb_3P_{16}B_{3.2}Si_{0.5}$), resulting in its negligible contribution to the detected surface chemical states.

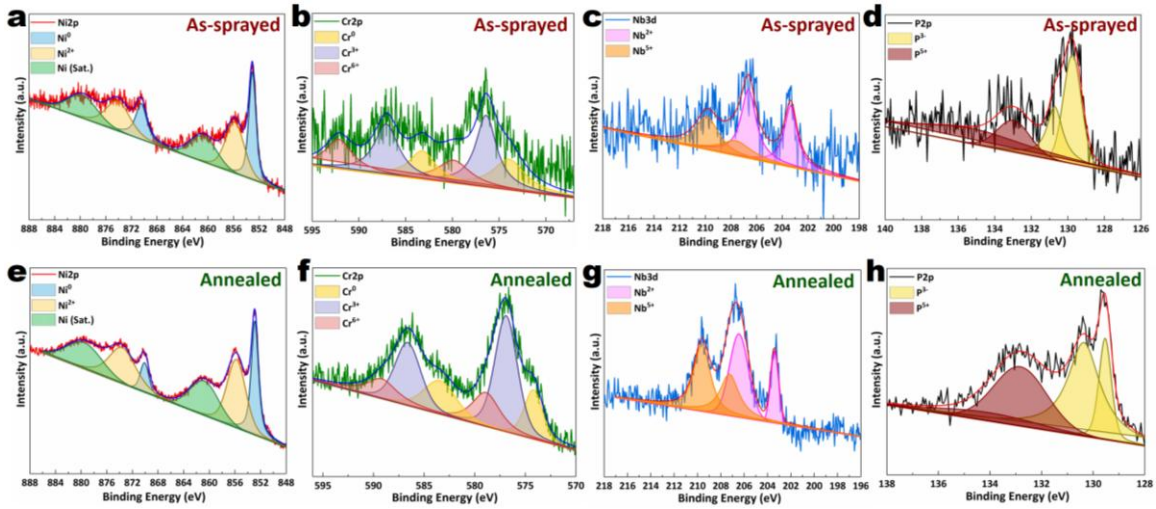


Fig. 8. XPS spectra of the oxidized worn surfaces of the fine-grained $Ni_{68.6}Cr_{8.7}Nb_3P_{16}B_{3.2}Si_{0.5}$ coatings after wear testing at room temperature: as-sprayed coating: **(a)** Ni 2p, **(b)** Cr 2p, **(c)** Nb 3d, and **(d)** P 2p spectra; and annealed coating: **(e)** Ni 2p, **(f)** Cr 2p, **(g)** Nb 3d, and **(h)** P 2p spectra.

Fig. 9 summarizes the relative fractions of oxide and phosphide species of Ni, Cr, Nb, and P in the worn surfaces of the as-sprayed and annealed coatings, quantified from fitted XPS spectra. The partially oxidized worn surface of the as-sprayed coating contains higher fractions of oxides including Cr_2O_3, CrO_3, NbO, and P_2O_5 (13.8%, 8.8%, 3.8%, and 21.6%, respectively) and lower fractions of phosphide Ni_3P (12.8%) (Fig. 9(a)). Importantly, CrO_3 and NbO are thermodynamically and mechanically unstable under tribological conditions, while P_2O_5 is a highly hygroscopic, glassy oxide. The decomposition of CrO_3 and NbO into more stable oxides results in poor interfacial cohesion and facilitates spallation. Furthermore, P_2O_5 promotes fracture and material removal due to its low mechanical strength under tribological loading conditions [35]. In contrast, the worn surface of annealed coating displays a pronounced decrease in the oxide

fractions including Cr_2O_3, CrO_3, NbO, and P_2O_5 (11.3%, 5.0%, 2.5%, and 9.9%, respectively) and increase in the phosphide (Ni_3P) fractions (22.6%) (Fig. 9(b)). The existence of the hard Ni_3P phosphide phase on the surface promotes a controlled wear mechanism, resulting in reduced wear rates and improved tribological performance [36, 37].

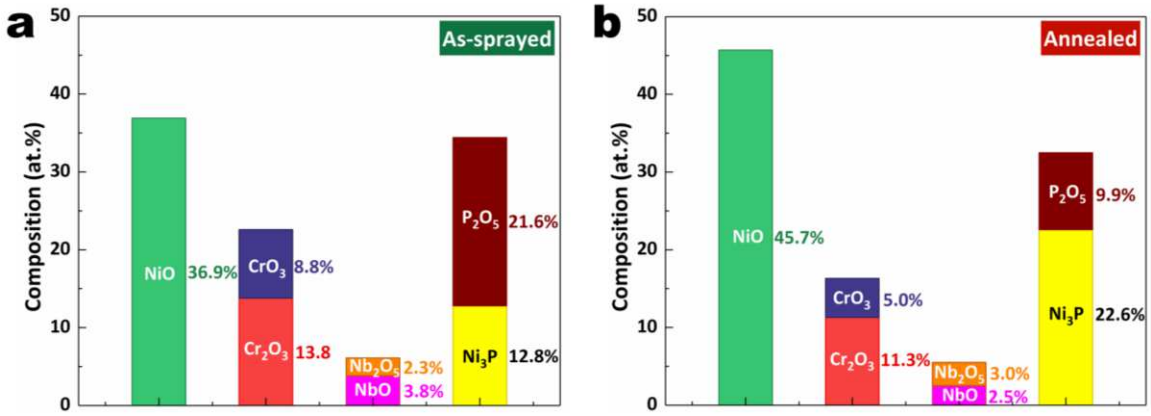


Fig. 9. Chemical compositions of the worn surfaces of the as-sprayed and annealed fine-grained $Ni_{68.6}Cr_{8.7}Nb_3P_{16}B_{3.2}Si_{0.5}$ coatings, determined from the XPS spectra.

3.5. Wear mechanism

Contrary to the literature, where high-temperature annealing typically promotes the precipitation of brittle intermetallic phases and/or excessively coarsens the grain size, in the present work, it results in a well-refined three-phase composite microstructure comprising ductile and hard phases. To demonstrate the superiority of the present annealed coating, a quantitative comparison with other annealed HVOF-sprayed metallic coatings, including FeMoCrYCB [38], CrAlTiN [39], NiCr-WC-Co [40], Cr_3C_2-25NiCr [41], CoMoCrSi [42], and NiCrBSi [43], was carried out and the obtained results are presented in Fig. 10. The present annealed coating exhibits the lowest wear rate among all the reference coatings reported in the literature. This significant improvement in wear resistance is primarily attributed to annealing-induced phase transformation along with significant (51%) reduction in intersplat density.

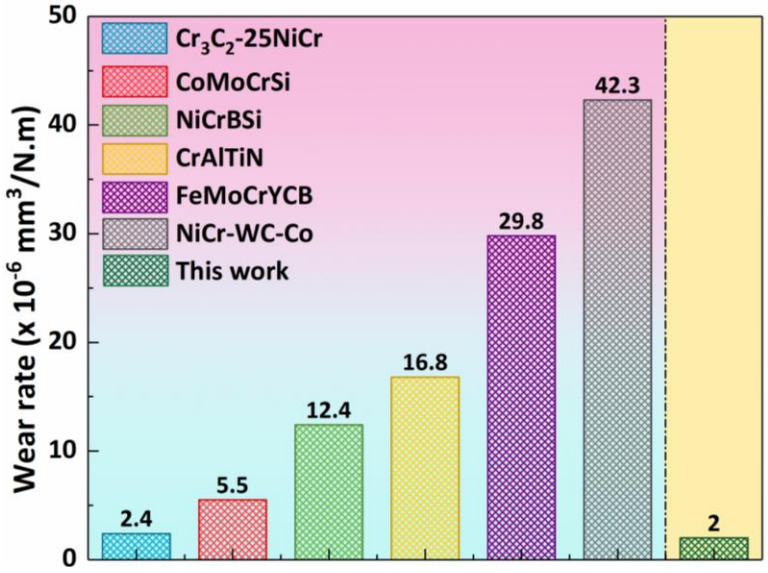


Fig. 10. Comparative plot of the present annealed coating with annealed FeMoCrYCB [38], CrAlTiN [39], NiCr-WC-Co [40], Cr_3C_2-25NiCr [41], CoMoCrSi [42], and NiCrBSi [44] amorphous coatings reported in the literature.

The annealing-induced phase transformation significantly modifies the tribological behavior of the fine-grained Ni-based coating. The wear response of the as-sprayed coating is dominated by its brittle microstructure, consisting of ~71 vol% FCC $Mg_6Cu_{17}Si_7$-type phase and ~14 vol% tetragonal Ni_3P phase (Fig. 2(a)) along with higher intersplat density (0.088 ± 0.004 μm^{-2}) (Fig. 1(c)). Owing to the limited plastic deformability of these phases and the stress-concentrating effect of intersplat and phase boundaries, contact stresses cannot be effectively accommodated, resulting in crack initiation and preferential propagation along intersplat and phase boundaries during sliding (Fig. 7(c)) [45]. The resulting fragmentation generates hard wear debris that becomes entrapped at the contact interface, acting as third-body abrasive particles and causing severe ploughing, cutting, delamination, and material spallation (Fig. 6(c)). Simultaneously, frictional heating promotes the formation of oxide blocks on the worn surface (Figs. 6(e) and 7(e)), which further contribute to wear damage and material removal [46]. Consequently, the wear mechanism

in as-sprayed coating involves severe abrasive wear, brittle fracture-induced delamination, and oxidative wear, resulting in a high wear rate.

In contrast, the superior wear resistance of the annealed coating is attributed to its refined three-phase microstructure, comprising ~51 vol% ductile Ni-based solid solution and ~43 vol% hard Ni_3P phase along with 51% reduced intersplat density. The ductile Ni-based solid solution matrix accommodates plastic deformation and enhances crack resistance, while the hard Ni_3P phase provides load-bearing capacity and resistance to surface deformation. Furthermore, the reduced intersplat density enhanced intersplat cohesion and reduced stress concentration sites, thereby suppressing crack initiation, splat delamination, and material removal. During sliding, dislocation motion within the Ni-based solid solution matrix is hindered by Ni_3P particles, promoting stress redistribution and restricting excessive plastic deformation, as discussed in our previous work [32]. As a result, the annealed coating exhibits a narrower wear track (Fig. 4(d)). Although the Ni_3P phase possesses limited deformability and is susceptible to crack initiation under high stress, the surrounding Ni-based solid solution arresting its shearing and suppresses crack propagation. Consequently, no cracks or spallation are observed on the worn surface. The presence of shallow grooves indicates that mild abrasive wear is the dominant wear mechanism, while the absence of pronounced oxide blocks and spallation zones suggests effective suppression of oxidative wear and delamination (Fig. 6(d) and (f)). Overall, the wear mechanism of the annealed coating is dominated by mild abrasive wear accompanied by limited plastic deformation, resulting in significantly lower wear rate.

The wear mechanisms of the as-sprayed and annealed coatings are schematically illustrated in Fig. 11. In as-sprayed condition (Fig. 11(a)–(b)), the coating consists of $Mg_6Cu_{17}Si_7$-type intermetallic phase (green patches) and Ni_3P phase (brown patches), separated by numerous intersplat

boundaries (dark grey arcs) and phase boundaries (dark grey lines). During sliding, cracks preferentially initiate and propagate along these weak regions, represented by red arcs and red lines, leading to material detachment and debris formation (small red dots). Oxidation within the wear track produces oxide blocks (large pink spots), while the entrapped debris causes severe abrasive wear and the formation of deep grooves (thick white lines) during sliding (Fig. 11(b)). In contrast, the annealed coating (Fig. 11(c)–(d)) consists of a Ni-based solid solution matrix (light grey patches) and Ni_3P phase (brown patches). Compared to the as-sprayed coating, the annealed coating contains both ductile and hard phases and fewer intersplat and phase boundaries, resulting in reduced crack formation and propagation and small amount of wear debris with no oxide blocks, and shallow abrasive grooves (thin white lines) during sliding (Fig. 11(d)).

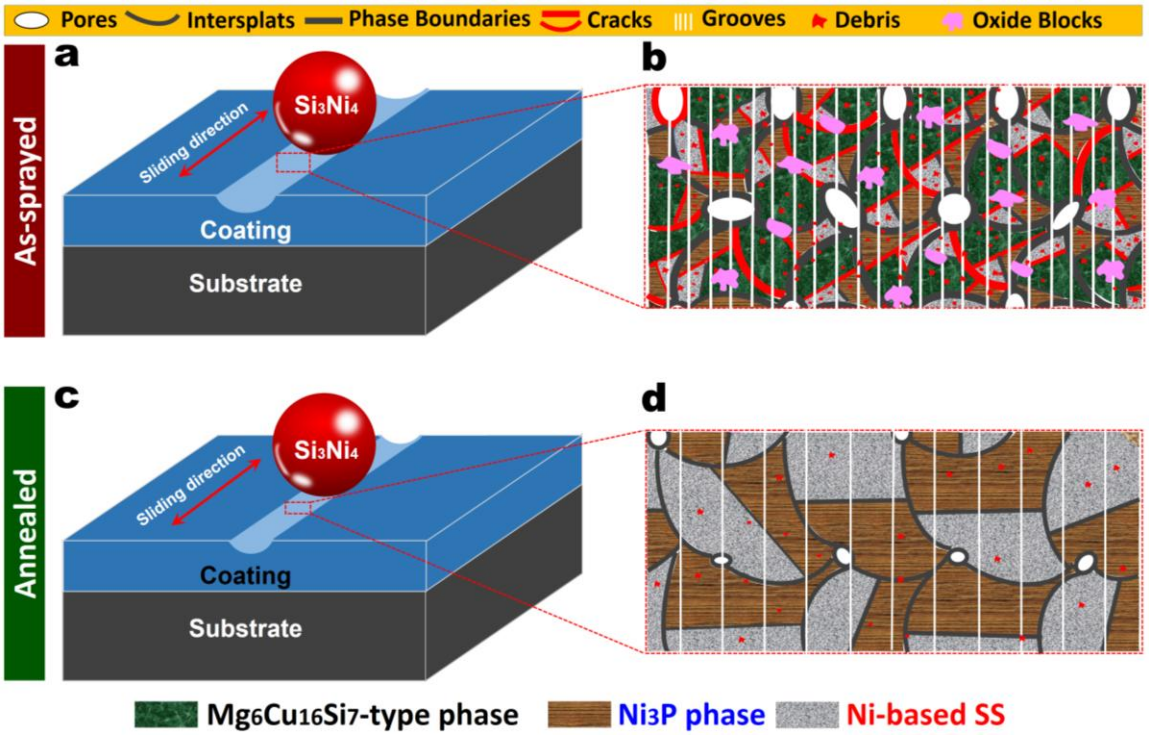


Fig. 11. Schematic representation of the wear mechanisms in the **(a)** and **(b)** as-sprayed and **(c)** and **(d)** annealed fine-grained $Ni_{68.6}Cr_{8.7}Nb_3P_{16}B_{3.2}Si_{0.5}$ coatings.

4. Conclusions

Through a controlled high-temperature annealing, we develop a highly wear-resistant $Ni_{68.6}Cr_{8.7}Nb_3P_{16}B_{3.2}Si_{0.5}$ coating with a dense fine-grained three-phase composite microstructure. In this microstructural configuration, the ductile Ni-based solid solution provides plastic deformation capability and crack resistance, whereas the hard Ni_3P and $NbNi_3$ phases contribute to enhanced load-bearing capacity. Annealing-induced reduction of intersplat density plays secondary role in improving the wear resistance by reducing stress concertation sites. Consequently, the annealed coating exhibits a 21% reduction in COF from 0.73 ± 0.05 (as-sprayed coating) to 0.43 ± 0.04 (annealed coating), and a substantial 89% reduction in wear rate from 17.79 ± 0.89 × 10^{-6} mm^3 $N^{-1}m^{-1}$ (as-sprayed coating) to 2.0 ± 0.10 × 10^{-6} mm^3 $N^{-1}m^{-1}$ (annealed coating), respectively, presenting enhanced friction and wear resistance. Overall, the annealed coating exhibits a mild abrasive wear with limited plastic deformation. The results demonstrate that careful alloy selection and precise annealing can overcome the intrinsic limitations of thermally sprayed AMCs, providing a practical route to produce fine-grained Ni-based coatings with superior tribological performance

Declaration of competing interest

The authors declare that they have no known competing financial interests or personal relationships that could have appeared to influence the work reported in this paper.

Acknowledgements

This work was financially supported by the National Natural Science Foundation of China (Grant Nos., 52441403, U23A20621, and 92366201) and the Foundation for Innovative Research Groups of the Natural Science Foundation of Hubei Province (Grant No. 2026AFA025). The authors are also grateful to the Analytical and Testing Center, Huazhong University of Science and Technology for technical assistance.

Data availability

Data will be made available on request.

References

[1] G. Shi, X. Yu, H. Meng, F. Zhao, J. Wang, J. Jiao, H. Jiang, Effect of surface modification on friction characteristics of sliding bearings: a review, Tribol. Int. 177 (2023) 107937.

[2] H. Li, Q. Zeng, M. Fan, Z. Pang, J. Wang, Y. Liang, Recent progress in high-temperature greases: Constitutive relationships, mechanisms, and applications, Friction 13 (2025) 9440951.

[3] J. Yu, X. Liu, Y. Yu, Z. Li, S. Xu, H. Li, P. Liu, L. Wang, Effect of HVOF spraying process on particle behavior of Fe-based amorphous alloy coatings, Therm. Spray Technol. 31 (2022) 2448-2462.

[4] Y.J. Sun, R. Yang, L. Xie, W.R. Wang, Y.B. Li, S.L. Wang, H.X. Li, J.M. Zhang, J.S. Zhang, Interfacial bonding mechanism and properties of HVOF-sprayed Fe-based amorphous coatings on LA141 magnesium alloy substrate, Surf. Coat. Technol. 426 (2021) 127801.

[5] L. Qiao, Y. Wu, S. Hong, J. Cheng, S. Zhu, Influence of annealing on microstructure and cavitation erosion resistance of iron-based metallic glass coatings synthesized by HVOF thermal spraying, Intermetallics 161 (2023) 107970.

[6] H. Nan, C. Li, K. Gao, X. Wang, Y. Tang, R. Tang, S. Kou, Enhancing the tribological properties of HVOF-sprayed Fe-based amorphous coatings via sealing with four different treatments, Tribol. Int. 217 (2026) 111612.

[7] T.-C. Chen, L.-W. Tsay, C.-C. Chou, S.-C. Hsu, Enhancing the corrosion–wear resistance of HVOF-sprayed Inconel 625 coatings via micro-shot peening, Surf. Coat. Technol. 517 (2025) 132801.

[8] C. Zhang, Q. Li, X. Zhang, G. Zhang, J. Li, Y. Huang, C. Chang, Effects of HVOF sprayed, laser cladding and laser remelted preparation process on wear and corrosion properties of Fe-based amorphous alloy coatings, Surf. Coat. Technol. 511 (2025) 132292.

[9] X. Wei, H. Hong, F. Dai, C. Zhang, Microstructure, fracture toughness and cavitation behavior of plasma-sprayed Fe-based amorphous coating by annealing treatment and laser remelting, Surf. Coat. Technol. 513 (2025) 132460.

[10] P. Zhang, H. Yan, P. Xu, Q. Lu, C. Li, Z. Yu, Influence of different annealing temperatures and cooling rates on amorphous and crystalline composite coating, Surf. Coat. Technol. 206(23) (2012) 4981-4987.

[11] J. Yang, M. Zhou, J. Yang, Relaxation and crystallization of amorphous FeCrAlTiMo coatings: Effects on mechanical properties and lead-bismuth eutectic corrosion resistance, Intermetallics 174 (2024) 108454.

[12] A.Q. Abbas, M.A. Hafeez, C. Zhang, M. Atiq-ur-Rehman, M. Yasir, Effect of crystallization on electrochemical and tribological properties of high-velocity oxygen fuel (HVOF)-sprayed Fe-Based amorphous coatings, Applied Chem 4 (2024) 270-281.

[13] J.B. Cheng, X.B. Liang, B.S. Xu, Devitrification of arc-sprayed FeBSiNb amorphous coatings: Effects on wear resistance and mechanical behavior, Surf. Coat. Technol. 235 (2013) 720-726.

[14] G. Liu, Y. An, J. Chen, G. Hou, J. Chen, Influence of heat treatment on microstructure and sliding wear of thermally sprayed Fe-based metallic glass coatings, Tribol. Lett. 46 (2012) 131-138.

[15] A.L. Greer, K.L. Rutherford, I.M. Hutchings, Wear resistance of amorphous alloys and related materials, Int. Mater. Rev. 47 (2002) 87-112.

[16] S. Weng, Z. Zhang, Y. Fu, L. Xue, P. Song, L. Shao, X. Liang, J. Cheng, B. Zhang, Effects of relaxation and nanocrystallization on wear and corrosion behaviors of Fe-based amorphous coating, Coatings 15(12) (2025) 1497.

[17] C. Sun, X. Zhou, C. Xie, L. Xu, R. Li, B. Liu, Formation of Al-based amorphous/nanocrystalline coatings by cold spraying, Surf. Coat. Technol. 389 (2020) 125644.

[18] Z. Huo, G. Zhang, J. Han, J. Wang, S. Ma, H. Wang, A review of the preparation, machining performance, and application of Fe-based amorphous alloys, Processes 10 (2022) 1203.

[19] C. Zhang, Q. Li, B. Xiong, G. Zhang, X. Ma, S. Guo, Z. Xu, F. Lu, J. Zhu, S. Yu, C. Chang, H. Li, Optimization of HVOF spraying parameters for enhanced Fe-based amorphous coatings: A taguchi approach, Intermetallics 173 (2024) 108419.

[20] C. Zhang, L. Xie, Q. Li, G. Zhang, C. Chang, H. Li, X. Ma, L. Liu, Influence of Ni, Al, W doping on microstructure, corrosion and wear resistance of HVOF spraying Fe-based amorphous alloy coatings, J. Mater. Res. Technol. 35 (2025) 1010-1029.

[21] H. Ma, D. Li, J. Li, Effect of spraying power on microstructure, corrosion and wear resistance of Fe-based amorphous coatings, Therm. Spray Technol. 31 (2022) 1683-1694.

[22] A. Meghwal, C. Schulz, C. Hall, E. Vogli, C.C. Berndt, A.S.M. Ang, Microstructural, mechanical and high-temperature tribological performance of Fe-based fully amorphous and amorphous/crystalline coatings, Surf. Coat. Technol. 475 (2023) 130114.

[23] R. Sun, L. Che, L. Xie, D. Zhang, Wear and corrosion resistant of NiFeSiBPNb amorphous alloy coatings sprayed by HVOF, Intermetallics 183 (2025) 108823.

[24] X.Z. Li, Y.T. Wang, G. Xu, M.L. Qin, S.N. Liu, R.S. Jiang, Z.D. Liu, Thick Ni based amorphous composite coating with good erosion wear resistance, Mater. Res. Innov. 18 (2014) S4-777-S4-781.

[25] D. Xu, G. Duan, W.L. Johnson, C. Garland, Formation and properties of new Ni-based amorphous alloys with critical casting thickness up to 5 mm, Acta Mater. 52 (2004) 3493-3497.

[26] C.L. Zhu, Q. Wang, Y.M. Wang, J.B. Qiang, C. Dong, Ni-based B–Fe–Ni–Si–Ta bulk metallic glasses designed using cluster line, minor alloying, and element substitutions, Intermetallics 18 (2010) 791-795.

[27] B. Shen, C. Chang, A. Inoue, Ni-based bulk glassy alloys with superhigh strength of 3800MPa in Ni–Fe–B–Si–Nb system, Appl. Phys. Lett. 88 (2006) 201903.

[28] J.K. Lee, D.H. Bae, S. Yi, W.T. Kim, D.H. Kim, Effects of Sn addition on the glass forming ability and crystallization behavior in Ni–Zr–Ti–Si alloys, J. Non-Cryst. Solids 333 (2004) 212-220.

[29] R. Li, Z. Li, Y. Zhu, K. Qi, Structure and corrosion resistance properties of Ni–Fe–B–Si–Nb amorphous composite coatings fabricated by laser processing, J. Alloys Compd. 580 (2013) 327-331.

[30] A.P. Wang, X.C. Chang, W.L. Hou, J.Q. Wang, Preparation and corrosion behaviour of amorphous Ni-based alloy coatings, Mater. Sci. Eng. A 449-451 (2007) 277-280.

[31] T. Zhang, A. Inoue, New bulk glassy ni-based alloys with high strength of 3000 MPa, Mater. Trans. 43 (2002) 708-711.

[32] M.A. Hafeez, P. Zhang, Z. Zhao, J.-C. Zhao, C. Zhang, L. Liu, High-temperature annealing enabled strong and tough Ni-based coating, Surf. Coat. Technol. 525 (2026) 133307.

[33] T. Zhang, A. Inoue, New bulk glassy Ni-based alloys with high strength of 3000 MPa, Material Transactions 43(4) (2002) 708-711.

[34] K. Bányai, M. Czagány, S. Kovács, G. Bognár, Characterisation of tribological properties and morphologies of Ni-P and Ni-B coatings, Lubricants 2025, p. 168.

[35] M. Woydt, Sub-stoichiometric oxides for wear resistance, Wear 440-441 (2019) 203104.

[36] A.A. Pauzi, M.J. Ghazali, W.F.H.W. Zamri, Fretting wear properties of Nimonic 263 at elevated temperatures, 2020.

[37] M.H. Attia, A. de Pannemaecker, G. Williams, Effect of temperature on tribo-oxide formation and the fretting wear and friction behavior of zirconium and nickel-based alloys, Wear 476 (2021) 203722.

[38] Y. Kang, Y. Chen, C. Yan, L. Kong, Influences of structural relaxation and crystallization on dry-sliding tribological behavior of Fe-based amorphous coating, Tribol. Lett. 69 (2021) 63.

[39] B. Huang, E.-g. Zhang, H.-m. Du, Q. Chen, D.-d. Liang, Q. An, Q. Zhou, Effects of annealing temperature on the microstructure, mechanical and tribological properties of CrAlTiN coatings, Surf. Coat. Technol. 449 (2022) 128887.

[40] A. Mazouzi, B. Djerdjare, S. Triaa, A. Rezzoug, B. Cheniti, S.M. Aouadi, Effect of annealing temperature on the microstructure evolution, mechanical and wear behavior of NiCr–WC–Co HVOF-sprayed coatings, J. Mater. Res. 35 (2020) 2798-2807.

[41] X. Liu, X. Zhao, F. Yang, Room-temperature and high-temperature wear behaviors of as-sprayed and annealed Cr_3C_2-25NiCr coatings prepared by high velocity air-fuel spraying, Coatings 2020, p. 1090.

[42] H. Guo, B. Li, P. Yan, Z. Wu, Microstructures, mechanical properties and tribological behaviors of HVOF-sprayed CoMoCrSi alloy coatings before and after 800 °C-annealed treatment, J. Alloys Compd. 909 (2022) 164662.

[43] Š. Houdková, E. Smazalová, The influence of high temperature exposure on the wear of selected HVOF sprayed coatings, Defect. Diffus. Forum. 368 (2016) 55-58.

[44] Š. Houdková, E. Smazalová, The influence of high temperature exposure on the wear of selected HVOF sprayed coatings, Defect Diffus. Forum 368 (2016) 55-58.

[45] J.A. Hawk, D.E. Alman, Abrasive wear of intermetallic-based alloys and composites, Mater. Sci. Eng. A 239-240 (1997) 899-906.

[46] K.S. Chan, Fracture toughness of multiphase intermetallics, MRS Online Proceedings Library 364 (1994) 469–480.